Energy materials

Enhanced surface-related ultraviolet–visible photoresponse in carbothermal ZnO nanowires by intertwined single-walled carbon nanotubes

Changsong Chen[1] , Yang Ma[1] , Jiang Chen[1] , and Haisheng San[1],*

[1] Pen-Tung Sah Institute of Micro-Nano Science and Technology, Xiamen University, Xiamen 361005, China

ABSTRACT

An intertwined single-walled carbon nanotubes (SWCNTs)/carbothermal ZnO nanowires (ZNWs) composite is synthesized using a facile ultrasonic stirring technology, which is deposited on Au-interdigitated electrodes for ultraviolet–visible (UV–Vis) photoresponse enhancement. It is found that the SWCNT attached on ZNW surface optimizes the surface-related chemical processes and provides effective carrier transport strategies, responsible for the improvement in photo-responsivity and photo-sensing speed. The UV–Vis absorption of ZNWs has been improved after compositing with the high-conductive SWCNTs, contributing to the significantly improved photo-conductance. The photodetector based on SWCNT/ZNW composites (CZWs) with an optimal SWCNT content of 0.1 wt% shows a 300% improvement in photocurrent density, a 200% improvement in responsivity, and a 400% improvement in on/off current ratio over the pure ZNWs-based device under a UV irradiation of 3.26 mW cm^{-2} and a bias voltage of 1.0 V. This synthetic method could be scaled up for large-scale fabrication of CZWs on substrate at low cost for practical photodetecting applications.

Introduction

Among the known one-dimensional (1D) nanomaterials, zinc oxide (ZnO) nanowire, as an emerging nanostructured functional material, has attracted significant attention for its three key advantages. First, it exhibits outstanding physical properties with large surface area, good crystal quality, and unique photonic properties [1–6]. Second, ZnO nanowires (ZNWs) have been successfully synthesized by several techniques, enabling their surfaces different chemical activities [7]. Finally, ZNWs are a low-cost material that can be solution-synthesized on a vast variety of substrates [5]. On account of these advantages, in the past few years, there has been an increasing interest in developing 1D ZNWs-based ultraviolet (UV) photodetectors and their potential applications in gas sensing, environmental monitors, and optical communications [4, 6, 8–10]. However,

the UV photodetectors based on pure ZNWs suffer from the weak photosensitivity due to the fast recombination of photo-excited electron–hole pairs (EHPs) in nanowires as well as the electron capture induced by oxygen molecules (O_2) chemisorption in the nanowire surface. Recently some strategies have been proposed to overcome these issues for photoresponse enhancement. A great amount of researches have focused on surface modification of the ZNWs nanostructure by compositing with low-dimensional nanomaterials, e.g., 1D single-walled carbon nanotubes (SWCNTs). Owing to good conductivity, superior chemical stability and high specific surface area [1–3, 11], SWCNTs have been regarded as a preferable candidate in materials modification. Chang et al. [12] and Ates et al. [13] presented high-photoresponse-aligned ZNW arrays-based photodetectors with a bottom electrode made of SWCNT monolayer. Vertically oriented ZNWs arrays can increase the photoresponse intensity and sensitivity through direct electron transport pathway beneficial to the reduction of EHPs recombination. Furthermore, it has been well established that heterojunction is formed at the interface between ZNWs and SWCNT [11], which can effectively separate the photo-generated EHPs and thus decrease the EHPs recombination. However, a main issue in such structure is that the SWCNT monolayer only contact nanowires in the nanowire ends [13], which results in a fact that 1D nanowires were not taken full use of their main merit of high specific surface area, and thus the devices would not realize its optimal performance. Therefore, that how to achieve the optimal structure is still an interesting and worth studying project when considering the composite between ZNWs and 1D nanomaterials.

Compared to the parallel-oriented ZNW arrays, the non-aligned ZNWs can be composited with SWCNTs for realizing more extensive and effective interface areas through a facile ultrasonic and stirring treatment in ZNWs suspension. This means that the non-aligned ZNWs combined with SWCNTs can be easily fabricated and assembled to the substrates in large-scale and low-cost preparation. While the SWCNTs show a promising strategy to enhance the photoresponse of ZNWs photodetectors, few studies on SWCNTs composited with non-aligned ZNWs have been systematically studied so far.

In this work, we present high-performance ultraviolet–visible (UV–Vis) photodetectors based on 1D-SWCNTs/1D-ZNWs composites (CZWs) attached on ceramics substrate with Au-interdigitated electrodes (IDEs). The composites of ZNWs and SWCNTs were obtained by ultrasonic stirring technology. The CZWs-based photodetectors incorporated with different SWCNT contents were fabricated for a systematic study on photoresponse enhancement in photo-absorption, photo-conductance, photo-gain and UV response speed.

Materials and methods

Synthesis of materials and fabrication of devices

Preparation of ZNWs was described in our previous work [14]. In brief, homogeneous mixture of commercial ZnO and graphite powder at a proportion of 1:3 was used as the source in a mixed atmosphere of oxygen and inert gas for a carbothermal reduction. The temperature was controlled to 800–1250 °C for 60 min to form crystallized wurtzite phase of ZNWs. The SWCNTs produced by high-pressure catalytic CO decomposition were purchased from Carbon Nanotechnologies Inc. As shown in Fig. 1, SWCNTs were mixed with ZNWs in ethanol solution, followed by an ultrasonication treatment for 150 min using an ultrasonic homogenizer (KQ-100KDE, China). To prevent heating during sonication, the bottle containing the sample solution was immersed in a bath of cold water. Then the sample solutions were magnetically stirred for 40 min at room temperature to form a homogeneous CZWs solution. Then the as-synthesized CZWs solution was added to the surface of Au-interdigitated electrodes (IDEs)/aluminum oxide (Al_2O_3) ceramics substrate, followed by air drying for 5 times to form an uniform CZWs film with an active area of 1.5×1.0 cm^2 as shown in Fig. 1. The Au IDEs containing 37 pairs of electrode fingers with finger thickness of 2–3 μm on ceramics substrates were fabricated by standard photolithography and lift-off process as shown in Fig. S1. To have the optimal photoelectric performance of the composites, the component proportion of CZWs solution was controlled to synthesize samples with different SWCNT contents of 0.05, 0.1, 0.2 wt%, respectively. For a comparative study, pure ZNWs samples were also fabricated and measured under the same experiment conditions (photographs of
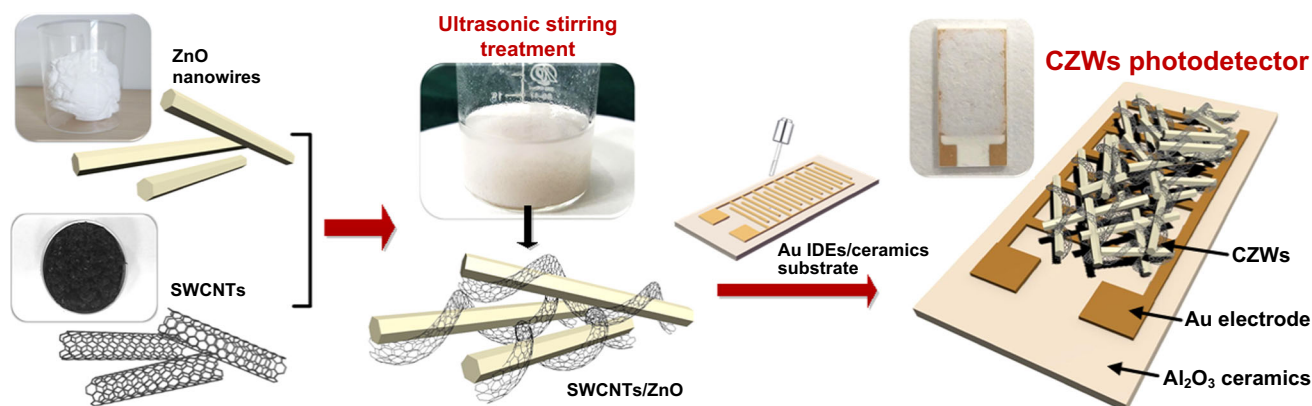
**Figure 1** Schematic illustration of fabrication processes of CZWs-based photodetectors and its photograph.

photodetectors based on ZNWs and CZWs are shown in Fig. S2).

Materials characterizations and device measurements

The morphology investigations were performed by a field emission scanning electron microscopy (FESEM, ZEISS microscope, Germany). An X-ray diffractometer (XRD, RigakuUltima IV, Japan) with a Cu-Kα radiation source was employed to analyze the crystallographic structure of the samples. The Raman spectra were measured by a spectrometer (Renishaw in via, UK) with a 532-nm laser as the excitation sources. The UV–Vis absorption spectral measurements of the samples were performed using a UV–Vis spectrophotometer (Cary 5000, USA). The photoresponse experiments were conducted using an electrochemical workstation (Chenhua CHI660E, China) at room temperature in a Faraday cage. Experimentally, a bias voltage or scanning voltage was applied to the device through two standard probes as shown in Fig. 2. A 3.08 W UV lamp (NICHIA NCSU033B, Japan) was used as the UV (365 nm) and visible irradiation source with tunable direct current power supply (Agilent E3631A, USA). Frequency signals of the UV light were modulated by a function waveform generator (Agilent 33250A, USA).

Results and discussion

Figure 3a, b shows top-view and magnified FESEM images of the 1D ZNWs, respectively. The super-long ZNWs are observed to interlaced disorderly each
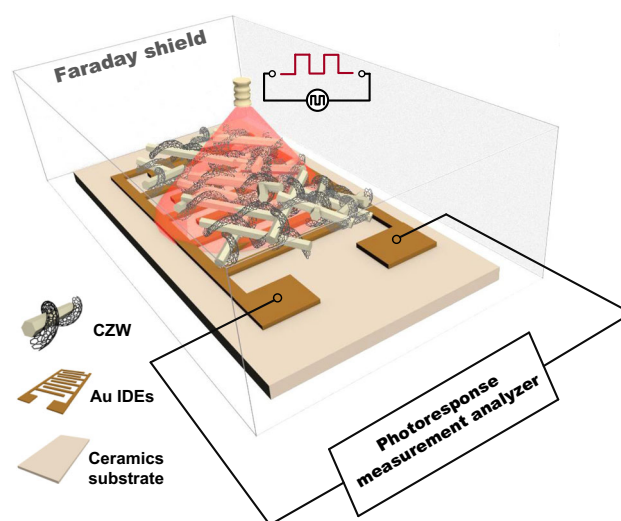
Figure 2 Schematic structure of CZWs-based UV photodetectors and its measurement system.

other with diameter of 80–200 nm and length of 2–20 μm. High magnification image (Fig. 1b) shows the carbothermal ZNWs have crystallized hexagonal morphology. The ultrahigh aspect ratio of the nanowires is beneficial to loading of modified materials and full absorbance of UV irradiation. In addition, the long nanowires can easily overlap each other to form nanowire networks beneficial to the SWCNTs anchoring on nanowires. Figure 3c, d shows the SEM images of the CZWs composited SWCNT content of 0.1 wt% (CZWs@0.1) before and after ultrasonic stirring treatment, respectively. (The optimal content is determined according to the results shown in Fig. 5.) As compared with Fig. 3c, the 1D SWCNTs are clearly observed to intertwine with the interlaced ZNWs after ultrasonic treatment and magnetic stirring, forming a 3D carbon nanotube-ZnO nanowire
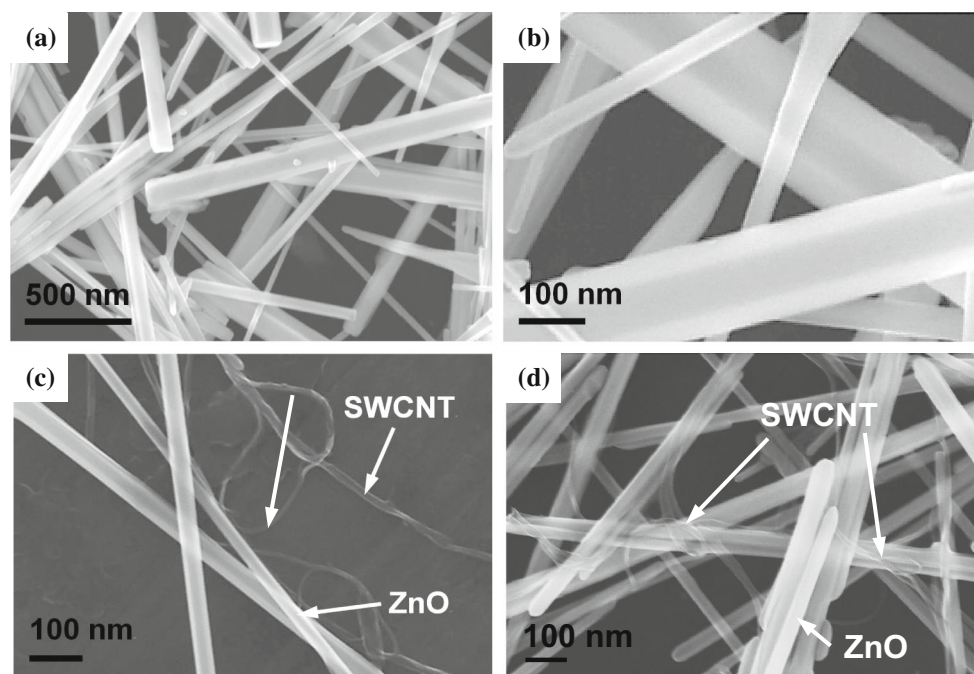
Figure 3 **a** Top-view and **b** magnified FESEM images of carbothermal ZNWs and FESEM images of SWCNTs/ZNWs **c** before and **d** after ultrasonic stirring treatment.

structure. Meanwhile, the long SWCNTs wrap around on ZNWs closely and make an interconnection between individual nanowires, which create a conductive network to provide abundant pathways extended in all directions for carrier transport.

The crystal structure and orientation of the samples were determined by X-ray diffraction study. As shown in XRD spectra of the pure ZNWs and CZWs@0.1 (see Fig. 4a), the ZnO nanowires possess standard hexagonal wurtzite ZnO structure (JPCDS 36-1451) in this study, which is in accord with the morphology features observed in Fig. 3. There is no new diffraction peak observed in CZWs, implying that the introduction of SWCNTs did not change the crystal structures of ZnO nanowires. The Raman spectra of the pure ZNWs and the CZWs are presented in Fig. 4b. The Raman frequencies of all of the peaks were extracted by Lorentzian fits and are assigned according to Ref [15–18] and listed in Table S1. Raman spectrum of SWCNTs possesses several main characteristic bands, i.e., a RBM band at $\sim 155 \text{ cm}^{-1}$, a M band observed at $\sim 1744 \text{ cm}^{-1}$, and the G band including a G^- band at $\sim 1552 \text{ cm}^{-1}$ and a G^+ band at $\sim 1584 \text{ cm}^{-1}$ [19]. Besides the broadened and flat M band, the intensity ratio I_G/I_D is calculated to be ~ 6.11, and the G^- band and G^+ band have similar intensities. All these features in

band structure and location agree well with the previous experimental findings for metallic characteristics of the SWCNTs, which means that carriers can be fast transported in nanostructures [20].

To study the effect of loading SWCNTs on UV absorption of the CZWs, UV–Vis spectra of the pure ZNWs and as-prepared composites are compared in Fig. 4c. All the samples show strong absorption for UV region, and the CZWs also exhibit enhanced absorption over a broad region from 300 to 600 nm as compared with the pure ZNWs. The CZWs with 0.1 wt% SWCNTs loaded exhibit a maximum absorption in UV region, showing a 7.5% higher absorbance than that of the pure ZNWs at wavelength of 365 nm. Such an enhanced absorption in both UV and visible regions is attributed to the increase in the surface charge of ZnO as well as the modified excitation formation induced by SWCNTs upon UV irradiation [21]. It is considered that the excessive content of SWCNTs composited into the ZNWs would induce immoderate light scattering and lead to reduction in photo-adsorption [14]. In contrast, the composite with higher SWCNTs loading (e.g., 0.2 wt% SWCNT content) shows an absorption decrease rather than further improvement as shown in Fig. 4c.
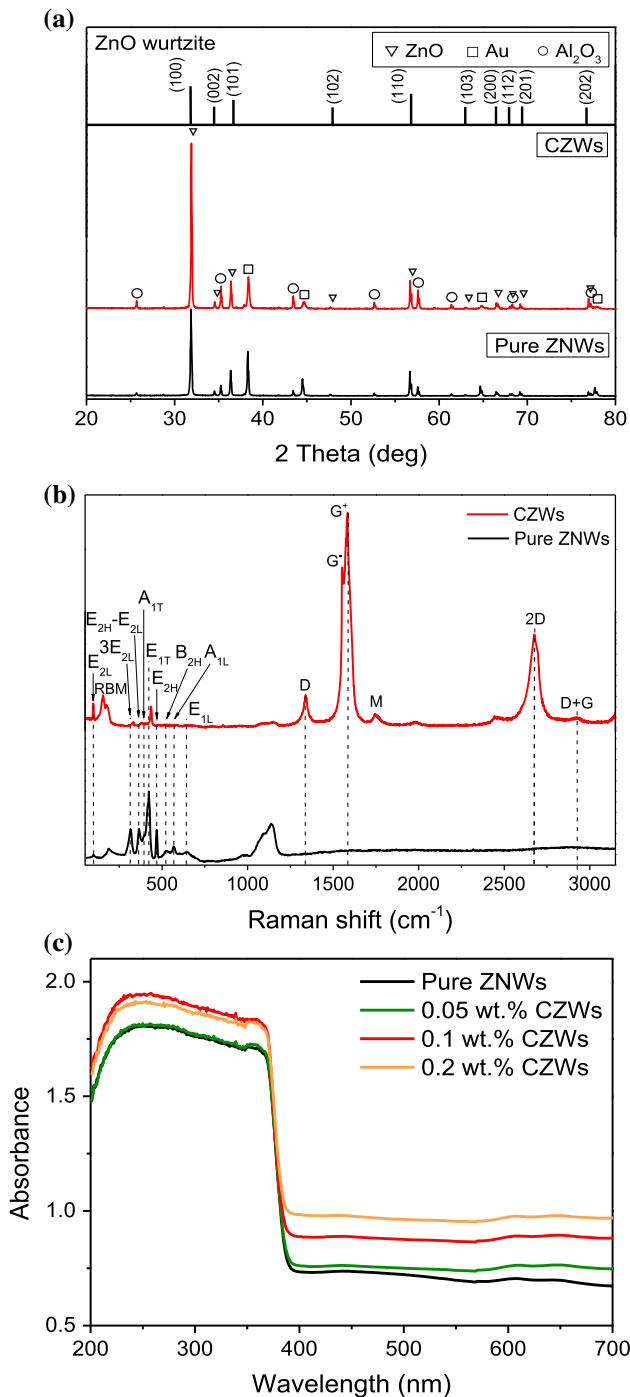
Figure 4 **a** XRD spectra and **b** Raman spectra of CZWs@0.1and pure ZNWs; **c** UV–Vis spectra of pure ZNWs and CZWs samples containing different SWCNT contents.

The photoresponse performances of the ZNWs before and after composited with SWCNTs were studied systematically. Figure 5a depicts the comparative current versus voltage (I–V) characteristics of the photodetectors based on pure ZNWs and

CZWs@0.1 in dark and under UV irradiation. Without irradiation, there is no appreciable change for the I–V curves of the photodetector before and after composited with SWCNTs. In contrast, with a UV irradiation, the device with SWCNTs exhibits a significant increase in I–V curve slope, indicating an enhanced photo-conductance in comparison with the pure ZNWs-based one. In order to determine the optimal SWCNT loading content for UV photoresponse enhancement, I–V characteristics of the photodetectors containing different content of SWCNTs, e.g., 0.05, 0.1, 0.2 wt%, were investigated for a comparison. As shown in Fig. 5b, under UV irradiation of 2.90 mW cm^{-2}, the CZWs@0.1-based photodetector shows the highest photo-conductance among the devices. With the increase in carbon nanotubes loading (e.g., 0.2 wt% SWCNTs), the I–V slope of composite would decrease due to the reduction in UV absorption of the sample, which can be confirmed from Fig. 4c.

Figure 5c shows the time-dependent photoresponses of the photodetectors under 3.26 mW cm^{-2} of UV irradiation controlled by switching on/off cycles and at a bias voltage of 1.0 V. It is observed that the CZWs-based photodetectors show significant enhancement in photocurrents when compared with the pure ZNWs-based device, and the photodetector based on CZWs@0.1 generates the highest photocurrent density of 3.52 mA cm^{-2}. Furthermore, on/off current ratio ($\Delta I_d/I_d$) of the devices under variable irradiation intensities was investigated. Here, $\Delta I_{d} = I_{ph} - I_d$, and I_{ph} and I_d are the current when the UV irradiation is switched on and off, respectively. The current–time characteristics of the pure ZNWs- and CZWs@0.1-based photodetectors under variable irradiation at a bias voltage of 1.0 V are presented in Fig. S3a and S3c, respectively, and the calculated on/off current ratios are shown in Fig. 5d. The $\Delta I_d/I_d$ values of both types of photodetectors increase linearly with the increase in UV intensity in a wide range of 0.24–2.75 V. The $\Delta I_d/I_d$ value of the CZWs-based photodetector is observed to be 84052 when the UV power density reaches 3.26 mW cm^{-2}. This value is around 5.5 times as high as that of the pure ZNWs-based photodetector ($\sim$ 15420). In addition, it is found from the inset of Fig. 5d that CZWs-based device can achieve a detection with minimum $\Delta I_d/I_d$ value of 1.54×10^3 (or the photocurrent density of 0.044 mA cm^{-2}) upon the lowest power density of the UV lamp ($\sim$ 6 μW cm^{-2}). The gradual saturation
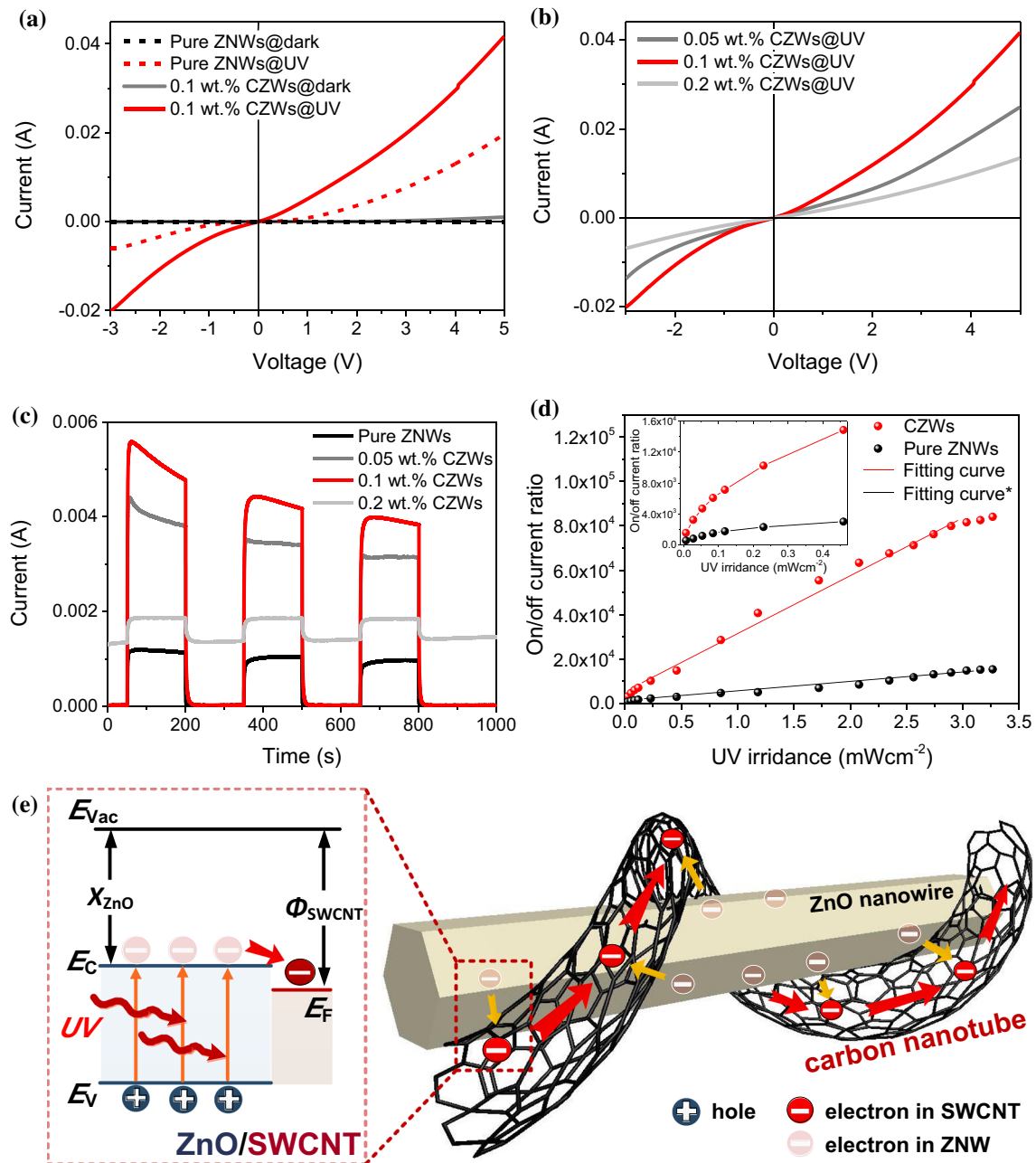
Figure 5 **a** I–V curves of pure ZNWs- and CZWs@0.1-based photodetectors in dark and under UV irradiation with a power of 2.90 mW cm^{-2}; **b** comparison of I–V curves of CZWs-based photodetectors with different SWCNT contents; **c** time-dependent photoresponses of photodetectors based on pure ZNWs and CZWs@0.1 under a UV intensity of 3.26 mW cm^{-2} with a bias of 1.0 V; **d** calculated on/off current ratio of the photodetectors based on pure ZNWs and CZWs@0.1. The inset is the magnification in low irradiance; **e** energy band diagram of SWCNTs/ZNWs system and carrier transport process in the interfacial region.

of $\Delta I_d/I_d$ in high UV irradiation region can be attributed to the flattening of the band bending and narrowing of the surface depletion layer at high irradiation intensity, resulting in a dynamic balance between generation and recombination of photo-

excited EHPs. This is also reported in other works of 1D ZnO-based photoresponse [9, 22].

The work mechanisms of the nano-composited SWCNT/ZnO structure in the photodetector can be understood from the energy band diagram. As

illustrated in Fig. 5e, the electron affinity of ZNW is 4.35 eV and the Fermi level of the SWCNT is 5.05 eV. The photo-generated electron is favorable to transfer from the conduction band of ZnO to SWCNT through the SWCNT/ZNW interface [23]. With an external electric field, these electrons will fast transfer from the metallic carbon nanotube to external circuit. This facilitates the separation of photo-excited EHPs, resulting in the enhancement in photocurrent of the photodetector.

The photoelectric characteristics are evaluated by responsivity (R_s) parameter, which is defined as:

$$R_s = \frac{I_{ph}}{P_{opt}}, \tag{1}$$

where P_{opt} is the specific UV intensity upon the active region of the devices. Figure 6a displays the R_s characteristics of the pure ZNWs- and CZWs@0.1-based photodetectors at a bias voltage of 1.0 V. The CZWs-based photodetector exhibits a

stable responsivity of 1.0 ($\pm$ 0.1) AW^{-1} under a wide range of UV irradiation (0.5–3.26 mW cm^{-2}), which is around 2.5 times as high as that of the pure ZNWs-based photodetector. It is considered that the photo-responsivity of photodetector is dominated by optical absorption capacity and photo-generated carrier lifetime of the composite. Since the SWCNT/ZnO composite can effectively suppress the recombination of EHPs, the lifetime and amount of carriers will be quite higher than that in pure ZNWs. In addition, time-dependent photoresponses of the two kinds of photodetectors at different bias voltage (V_b) were studied as presented in Fig. S3b and S3d, and the calculated R_s is depicted in Fig. 6b. It can be seen that R_s of the CZWs-based photodetector exhibits positive linear relations in a wider V_b range from 0.2 V to 2.5 V and exhibits a higher saturation value by 48.7% as compared with the pure ZNWs-based one.

Photoconductive gain (G_{ph}) and specific detectivity (D^*) are used to further assess photoresponse
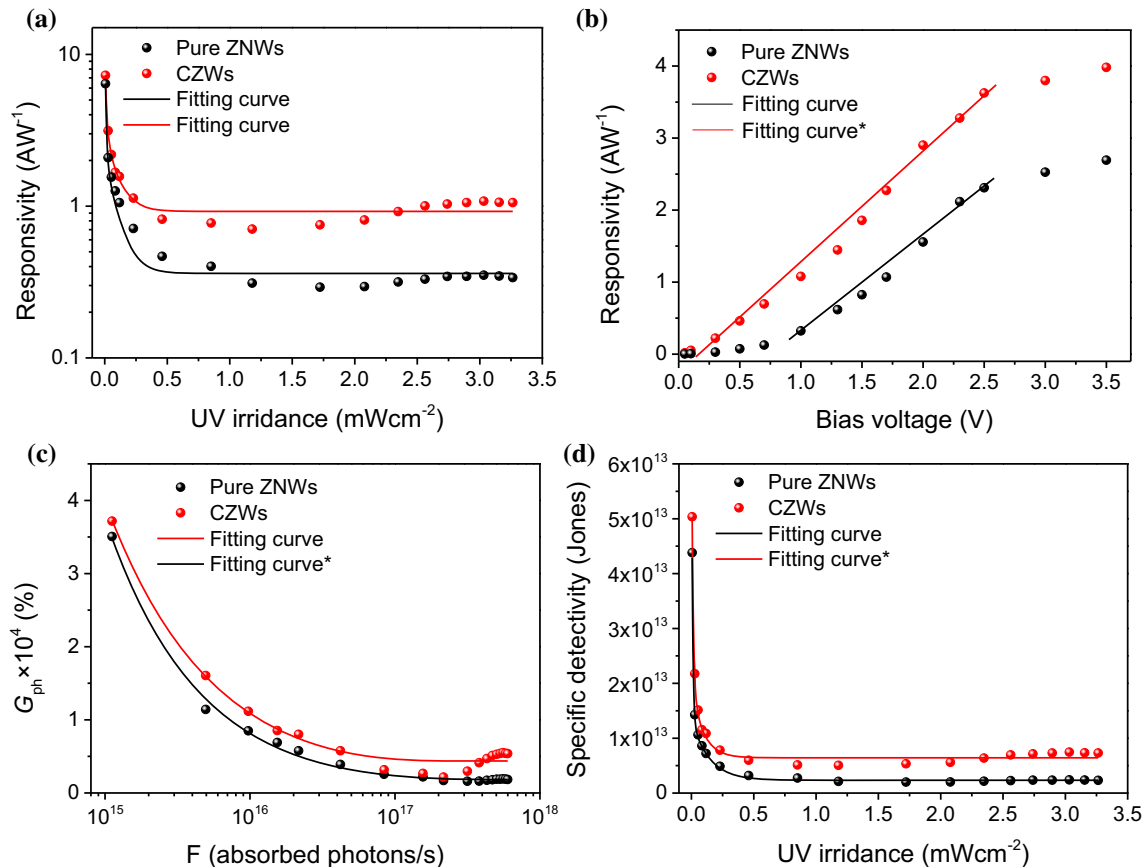
Figure 6 Dependence of photo-responsivity on **a** UV intensity and **b** bias voltage of the photodetectors based on pure ZNWs and CZWs@0.1 at a bias voltage of 1.0 V; **c** dependence of photoconductive gain on photon absorption rate of the two kinds of devices; **d** dependence of specific detectivity on UV intensity of the two kinds of devices.
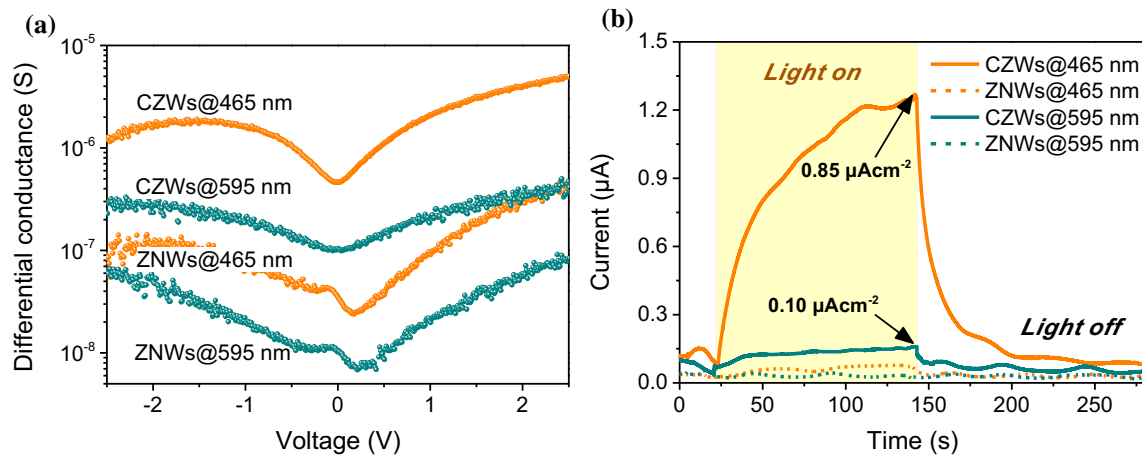
Figure 7 **a** Photo-conductance and **b** time-dependent photoresponse of pure ZNWs- and CZWs@0.1-based photodetectors under visible light at wavelengths of 465 and 595 nm.

properties of the devices. G_{ph} is defined as the number of electrons collected by electrodes induced by one incident photon, which is defined as:

$$G_{ph} = \frac{I_{ph}}{P_{opt}} \times \frac{h\upsilon}{e} = \frac{I_{ph}}{e} \times \frac{1}{F}, \qquad (2)$$

where $h\upsilon$ is the energy of the incident photon, and e is the electron charge. D^* determines how weak the light signal could be identified from the noise environment. Assuming that shot noise from the dark current mainly contributes to the total noise, the detectivity can be evaluated by the formula:

$$D^* = \frac{J_{ph}\sqrt{S}}{P_{opt}\sqrt{2eI_d}}, \qquad (3)$$

where J_{ph} is photocurrent density and S is the device area. Figure 6c shows dependence of G_{ph} on the photon absorption rate (F). It is found that photoconductive gains are 3.5×10^4 and 3.7×10^4 for pure ZNWs- and CZWs@0.1-based photodetectors when photon absorption rate is 10^{15}, respectively. With the increase in photon absorption rate, the G_{ph} present a decay trend, which is also reported in other works [24]. This can be explained by the shortening of the carrier lifetime caused by a manifestation of hole-trap saturation and the increased recombination rate at the high irradiance. Figure 6d depicts dependence of specific detectivity on UV intensity of these two kinds of devices. In a wide irradiance range, the CZWs-based photodetector shows an enhanced detectivity of $(7.0 \pm 0.3) \times 10^{12}$ Jones in a stable level by 204% over the pure ZNWs-based photodetector $((2.3 \pm 0.2) \times 10^{12}$ Jones). It is noticeable that the

CZWs-based photodetector exhibits a remarkable detectivity of 5.04×10^{13} Jones under a weak UV irradiation of $\sim 6\ \mu W\ cm^{-2}$, which is one orders of magnitude higher than that of the previous report [25].

Photoresponse characteristics of the devices at visible wavelengths were also investigated. Under visible light of 2.68 mA cm^{-2} at 465 and 595 nm, the CZWs@0.1-based photodetector shows significantly enhanced electric conductance, which is one order of magnitude higher than that of pure ZNWs-based device, as shown in Fig. 7a. Figure 7b shows the time-dependent photoresponses of the photodetectors at a bias voltage of 1.0 V and under visible light. The CZWs-based photodetectors show typical photoresponse behaviors with a photocurrent density of 0.85 $\mu A\ cm^{-2}$ under irradiation of 465 nm. It is found that the photoresponse intensity at wavelength of 595 nm is clearly weaker than that under the UV light, but the CZWs device exhibits higher photocurrent than that of the pure ZNWs-based device. This indicates that the introduction of SWCNTs promotes its visible-light detectivity. Compared with ZNWs, this SWCNT/ZnO composite structure is promising for development of broadband photodetector.

The high response speed of photodetector plays a crucial role in practical applications such as imaging, optical switching, and optical communications. Figure 8a, b exhibits the fast transient response of the photodetectors. For ZNWs and CZWs devices, the rise time (t_r) are 2.42 and 1.99 s, respectively, and the fall-time (t_d) are 0.20 and 0.39 s, respectively. Surface-
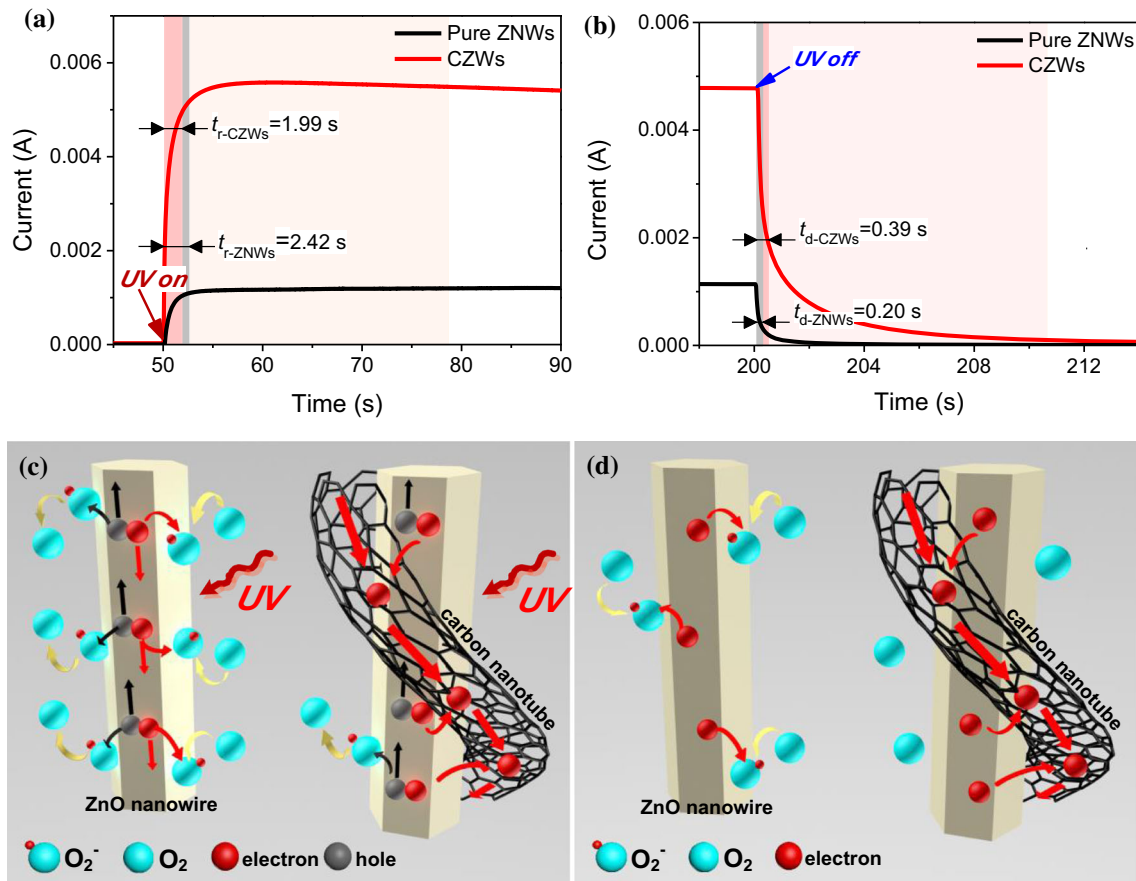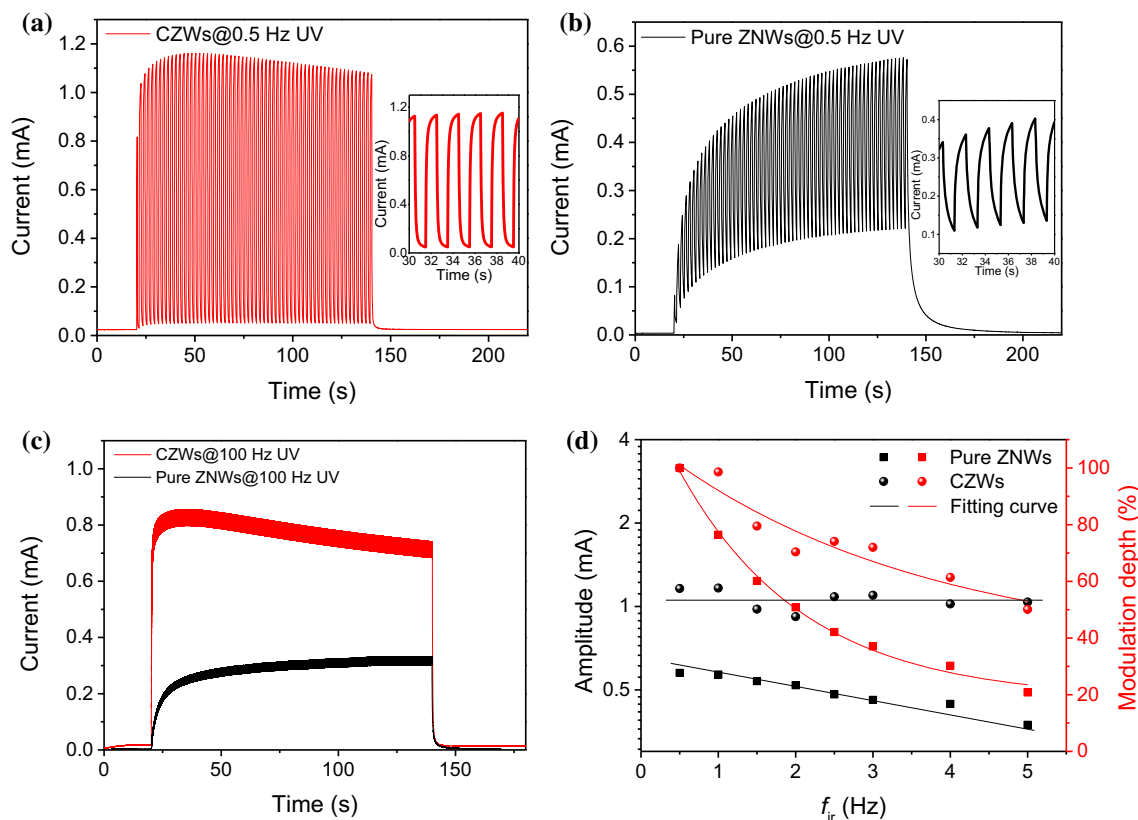
Figure 8 Time-dependent photoresponse **a** rise process and **b** decay process of the pure ZNWs- and CZWs@0.1-based photodetectors. Schematic diagram of surface-state-related chemisorption and photo-desorption processes in pure ZNWs and CZWs **c** with and **d** without UV irradiation.

state-related chemisorption and photo-desorption of oxygen in SWCNT/ZnO interface will be responsible for the enhancement of photo-sensing speed of the CZWs-based device. It has been well established that the transient response of ZnO-based UV detectors consisted of a fast process due to the photo-excited EHPs generation and a slow process due to the oxygen chemisorption in the ZnO surfaces [26]. As shown in Fig. 8c, oxygen molecules can be easily adsorbed onto the exposed surface of ZnO by capturing free electrons from the ZnO ($[O_2(g) + e^- \rightarrow O_2^-(ad)]$), which results in the decrease in conductivity of ZnO. With an UV irradiation, the photo-induced holes will be captured by the surface states of ZnO ($[O_2^-(ad) + h^+ \rightarrow O_2(g)]$). In contrast, this process is weakened in CZWs because the electrons prefer to be transferred through the SWCNTs rather than captured by oxygen. When the UV light is off, oxygen molecules will be re-adsorbed onto the

exposed surface of ZNWs. The photo-generated electrons will keep contributing to the photocurrent until they are captured in the oxygen chemisorption process. In CZWs, the composited carbon nanotubes in ZNWs would hinder this process, as shown in Fig. 8d. As a result, the CZWs-based photodetector would take longer time to recover than the pure ZNWs-based device.

Figure 9a, b exhibits the time-dependent photoresponses of pure ZNWs- and CZWs@0.1-based photodetectors under 3.26 mW cm^{-2} of UV irradiation with an on/off frequency (f_{ir}) of 0.5 Hz, respectively. It is seen that there are clear modulated-signals in amplitude envelopes of both kinds of photodetectors. The CZWs-based photodetector exhibits the complete modulated-waveform and good photoresponse speed, while the pure ZNWs-based device shows a considerable reduction in peak-to-peak amplitude (I_{P-P}). The I_{P-P} in peak envelope of the CZWs-based

Figure 9 Time-dependent photoresponses of **a** CZWs@0.1-based and **b** pure ZNWs-based photodetector under 3.26 mW cm^{-2} of UV irradiation with an on/off frequency of 0.5 Hz. The insets shows the magnified figures; **c** Comparison of time responses of these two kinds photodetectors under a UV flash irradiation of 100 Hz; **d** dependence of photocurrent amplitude and modulation depth on UV irradiation frequency of these two kinds photodetectors.

device implies a much better relative-balance-ratio ($I_{p-p,max}/I_{max} \times 100\%$) than that of ZNWs-based one (98.2% for CZWs and 60.7% for ZNWs). Since the speed of carrier movement in CZWs is fast and thus can keep up with the on/off frequency of the UV irradiation, the CZWs-based device exhibits excellent modulation response. Furthermore, as the UV irradiation frequency is modulated to 100 Hz, the CZWs-based device still exhibits a very fast photoresponse speed and a long-term repeatability with about 10.0% of relative-balance-ratio, and the photocurrent amplitude of the device reached 0.57 mA cm^{-2}, which is 2.3 times as high as that of the pure ZNWs-based one (see Fig. 9c). Based on above test method, dependences of photocurrent amplitude and modulation depth on UV irradiation frequency were studied as presented in Fig. 9d. With a UV irradiation of 3.26 mW cm^{-2} and a bias voltage of 1.0 V, the pure ZNWs-based photodetectors exhibit a declining trend in photocurrent amplitude with the increase in irradiation frequency. By contrast, the CZWs-based

photodetector shows a stable photoresponse value with photocurrent amplitudes of 1.0 ($\pm$ 0.2) mA under UV irradiation frequency of 0.5–5 Hz. In addition, modulation depth $M(f_{ir})$ of the photodetectors was also calculated by:

$$M(f_{ir}) = \frac{I(f_{ir})_{p-p}}{I(0.5Hz)_{p-p}} \times 100\%, \qquad (4)$$

where $I(f_{ir})_{p-p}$ is the peak-to-peak value of the photocurrent at UV irradiation frequency (f_{ir}), and the modulation depth at 0.5 Hz frequency is determined as 100%. It can be seen from Fig. 8d that modulation depth for the pure ZNWs-based photodetector declines to 20% at UV irradiation frequency of a 5 Hz, while the CZWs-based photodetector exhibits a modulation depth is more than 50%. It is suggested that the SWCNTs play important role in optimizing surface-related photoelectric behaviors and channels for fast carrier transport, which facilitates the enhanced UV modulation response.

Conclusion

We fabricated a high-performance UV–Vis photodetector based on SWCNTs/ZNWs composite coated on Au IDEs/ceramics substrates. ZNWs were successfully synthesized through a carbothermal reduction method and composited with SWCNTs via an ultrasonic stirring technology. The photodetectors can be prepared in large scale for practical applications through the solution method. The CZWs with 0.1 wt% SWCNT content loaded have the optimal photo-absorption and photoresponse properties. In comparison with the pure ZNWs-based photodetector, CZWs@0.1-based device exhibits enhanced photoresponse with a photocurrent density of 3.52 mA cm^{-2}, a responsivity of 1.06 AW^{-1}, and an on/off current ratio of 8.4×10^4, under a UV irradiation of 3.26 mW cm^{-2}. The CZWs-based photodetector also shows fast response speed and high modulation depth upon modulated UV irradiation. Theory analysis indicates that the CZWs-based photodetector provides multiple strategies for photoresponse enhancement by suppressing carrier recombination and surface-related effects in ZNWs. The excellent photoresponse performances of the CZWs provide a promising strategy for developing the practical and economical UV photodetectors.

Compliance with ethical standards

Conflict of interest The authors declare that they have no conflict of interest.

Electronic supplementary material: The online version of this article (https://doi.org/10.1007/s10853-018-2525-8) contains supplementary material, which is available to authorized users.

References

[1] Tsukazaki A, Ohtomo A, Onuma T et al (2005) Repeated temperature modulation epitaxy for p-type doping and light-emitting diode based on ZnO. Nat Mater 4:42–46

[2] Wan Q, Li QH, Chen YJ et al (2004) Fabrication and ethanol sensing characteristics of ZnO nanowire gas sensors. Appl Phys Lett 84:3654–3656

[3] Law M, Greene LE, Johnson JC, Saykally R, Yang P (2005) Nanowire dye-sensitized solar cells. Nat Mater 4:455–459

[4] Wang ZL, Song J (2006) Piezoelectric nanogenerators based on zinc oxide nanowire arrays. Science 312:242–246

[5] Zhang H, Babichev AV, Jacopin G et al (2013) Characterization and modeling of a ZnO nanowire ultraviolet photodetector with graphene transparent contact. J Appl Phys 114:234505–234513

[6] Panda D, Tseng TY (2013) One-dimensional ZnO nanostructures: fabrication, optoelectronic properties, and device applications. J Mater Sci 48:6849–6877. https://doi.org/10.1007/s10853-013-7541-0

[7] Elias J, Tenazaera R, Wang GY, Lévyclément C (2008) Conversion of ZnO nanowires into nanotubes with tailored dimensions. Chem Mater 20:6633–6637

[8] Fu X-W, Liao Z-M, Zhou Y-B et al (2012) Graphene/ZnO nanowire/graphene vertical structure based fast-response ultraviolet photodetector. Appl Phys Lett 100:223114

[9] Dang VQ, Trung TQ, Kim DI et al (2015) Ultrahigh responsivity in graphene-ZnO nanorod hybrid UV photodetector. Small 11:3054–3065

[10] Bai Z, Fu M, Zhang Y (2017) Vertically aligned and ordered ZnO/CdS nanowire arrays for self-powered UV–visible photosensing. J Mater Sci 52:1308–1317. https://doi.org/10.1007/s10853-016-0426-2

[11] Zhang WD, Jiang LC, Ye JS (2009) Photoelectrochemical study on charge transfer properties of ZnO nanowires promoted by carbon nanotubes. J Phys Chem C 113:16247–16253

[12] Chang J, Khalid Najeeb C, Lee JH, Lee M, Kim JH (2011) High-performance photoresponse from single-walled carbon nanotube-zinc oxide heterojunctions. J Phys D Appl Phys 44:885–896

[13] Ates ES, Kucukyildiz S, Unalan HE (2012) Zinc oxide nanowire photodetectors with single-walled carbon nanotube thin-film electrodes. ACS Appl Mater Interfaces 4:5142–5146

[14] Chen C, Zhou P, Wang N, Ma Y, San H (2018) UV-assisted photochemical synthesis of reduced graphene oxide/ZnO nanowires composite for photoresponse enhancement in UV photodetectors. Nanomaterials 8:26–38

[15] Rajalakshmi M, Arora AK, Bendre BS, Mahamuni S (2000) Optical phonon confinement in zinc oxide nanoparticles. J Appl Phys 87:2445–2448

[16] Porto SPS, Tell B, Damen TC (1966) Near-forward raman scattering in zinc oxide. Phys Rev Lett 16:450–452

[17] Xing YJ, Xi ZH, Xue ZQ et al (2003) Optical properties of the ZnO nanotubes synthesized via vapor phase growth. Appl Phys Lett 83:1689–1691

[18] Özgür Ü, Alivov YI, Liu C et al (2005) A comprehensive review of ZnO materials and devices. J Appl Phys 98:041301–041403

[19] Dresselhaus MS, Dresselhaus G, Saito R, Jorio A (2005) Raman spectroscopy of carbon nanotubes. Phys Rep 409:47–99

[20] Silva KC, Corio P, Santos JJ (2016) Characterization of the chemical interaction between single-walled carbon nanotubes and titanium dioxide nanoparticles by thermogravimetric analyses and resonance Raman spectroscopy. Vib Spectrosc 86:103–108

[21] Liu X, Pan L, Zhao Q et al (2012) UV-assisted photocatalytic synthesis of ZnO–reduced graphene oxide composites with enhanced photocatalytic activity in reduction of Cr(VI). Chem Eng J 183:238–243

[22] Dang VQ, Trung TQ, Duy TL et al (2015) High-performance flexible ultraviolet (UV) phototransistor using hybrid channel of vertical ZnO nanorods and graphene. ACS Appl Mater Interfaces 7:11032–11040

[23] Robel I, Bunker BA, Kamat PV (2005) Single-walled carbon nanotube-CdS nanocomposites as light-harvesting assemblies: photoinduced charge-transfer interactions. Adv Mater 17:2458–2463

[24] Soci C, Zhang A, Xiang B et al (2007) ZnO nanowire UV photodetectors with high internal gain. Nano Lett 7:1003–1009

[25] Lee S-W, Choi K-J, Kang B-H et al (2016) Low dark current and improved detectivity of hybrid ultraviolet photodetector based on carbon-quantum-dots/zinc-oxide-nanorod composites. Org Electron 39:250–257

[26] Takahashi Y, Kanamori M, Kondoh A, Minoura H, Ohya Y (1994) Photoconductivity of ultrathin zinc-oxide films. Jpn J Appl Phys 33:6611–6615